Multistatic laser ranging simulations for improved orbit determination of space debris

Pascal Sauer [(1)], Alessandro Vananti [(1)], Thomas Schildknecht [(1)]

[(1)] Astronomical Institute University of Bern, Sidlerstrasse 5 3012 Bern Switzerland, Email: pascal.sauer@unibe.ch

ABSTRACT

Space debris laser ranging is a way to get high accuracy range information about a space debris object. Laser ranging in a bi-static configuration, where the sending and receiving station is not the same, has been experimentally demonstrated in 2013. The advantage of this technique is that only one station needs to be equipped with a high-power laser and other stations can observe the target in a passive receiving mode, leading to a better utilization of the network of laser ranging stations. Increasing the number of receiving stations to two or more (multi-static), can lead to an improved orbit determination accuracy. In this contribution we present a simulation framework, that is capable of generating realistic SDLR measurements and utilize different types of measurements like mono- and bistatic laser ranges or angular measurements to evaluate the orbit determination performance of different observation scenarios. In particular we investigate how flyover geometries and the placement of receiving stations influences the estimation of different orbital parameters.

1 Introduction

Space Debris Laser Ranging (SDLR) enables high precision range measurements to resident space objects (RSO). A laser ranging station sends short pulses of light to an RSO of interest, the pulses get diffusely reflected at the object and the time of flight between sending and receiving epoch is measured. In comparison to Satellite laser ranging (SLR), most space debris objects are not equipped with retroreflectors, which are able to reflect light back to the sending ground-station. SDLR relies instead on diffuse reflection of laser pulses from the objects structure. As diffusely reflected photons are scattered in a multitude of directions, this enables the photons being detected by more stations than just the observer station. Bi-static laser ranging with one sending and another receiving station was first demonstrated in 2013 [1], and has been shown to decrease orbit uncertainties [2-4]. As SDLR requires the use of special laser systems with pulse energies high enough to utilize the diffuse reflections from the RSO structure, bi- and multistatic observations are an efficient way to use the limited SLR stations resources to its maximum potential. Using only a single pass, a full orbit determination is not guaranteed for a monostatic configuration [2], but can be improved by reducing the number of estimated parameters, or adding additional measurements, e.g. angular measurements from the encoders of the telescope [5]. It has been shown, that while single laser ranging passes usually don't allow full estimation of all orbital parameters, adding at least one bistatic receive station can lead to being able to estimate all orbital parameters [2]. Multiple receive only stations can further decrease the estimation parameter uncertainties with diminishing returns [2, 3], i.e. each additional station decreasing the uncertainty by smaller amounts. A tracking campaign of the defunct ENVISAT was described in [4], which confirmed, that bistatic SDLR can decrease the orbit uncertainties enough for "blind" tracking, i.e. tracking without the aid of an optical tracking-camera, which is essential during daytime.

2 Methods

In this simulation study, different bi- and multistatic orbit determination scenarios are examined by a simulation based on the Orekit framework. Orekit [6] is a Java based, open-source flight dynamics package developed and managed by CS Group. It features spacecraft propagation, frame handling and orbit determination capabilities. The framework was chosen because of the open source nature of the source code, already implemented support of multiple orbit determination tools, including the necessary observation types as well as support through an active community forum. The Orekit library is available in a Python-wrapper, which enables the usage of the Python data-management and visualization ecosystem.

Proc. 9th European Conference on Space Debris, Bonn, Germany, 1–4 April 2025, published by the ESA Space Debris Office
Editors: S. Lemmens, T. Flohrer & F. Schmitz, (http://conference.sdo.esoc.esa.int, April 2025)

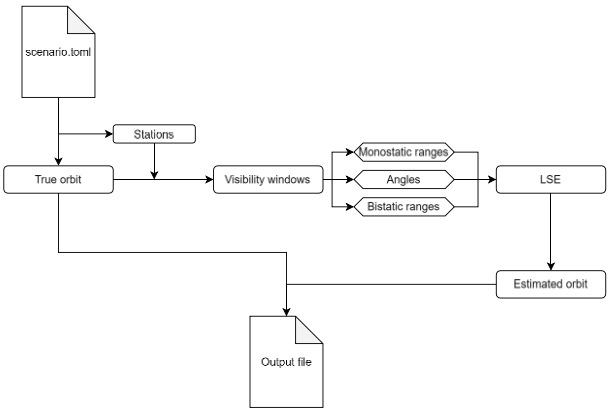

Figure 1: Schematic simulation workflow

A schematic visualizing the simulation structure displayed in Fig. 1. Based on the "true" orbit, specified in an initial configuration-file, the position of the RSO is propagated and visibility windows of the stations calculated. Next, measurements of the stations are generated. For the presented scenarios only one station is considered to be equipped with a space debris laser and therefore a sending station. Sending stations can contribute monostatic ranges, where the sending station receives their own laser pulses, and angular measurements (Azimuth and Elevation angles), which are modelled after encoder values, which can be used to increase observability [5]. All other stations are considered as receive only, which contribute bistatic measurements. The noise distribution is assumed to be gaussian. After generation of all measurements is completed, they are added to a Least-Squares Estimator (LSE) orbit determination algorithm. The LSE tries estimating an orbit based from initial orbital parameters provided in the configuration file, utilizing a Gauss-Newton optimization algorithm, which uses a QR decomposer to solve the system of normal equations. A convergence-checker evaluates the root-mean-squares (RMS) of the residuals at each iteration. Convergence is achieved if the RMS is not changing above a threshold given in the configuration file. The resulting orbital state, along with its covariances is saved to an output file for further analysis. As the measurements are based on a random number generator, the simulation is wrapped in a Monte-Carlo layer. The simulations are repeated while varying the seeds of the random number generator of each run. The number of these Monte-Carlo runs is set to 100 by default.

3 Results and Discussion

The following presented scenarios consider an object in low earth orbit (800 km) with a low eccentricity (10^{-4}). Three different inclinations are considered (98°, 80°, and 50°) to produce different flyover geometries. Sixteen receive-only stations are placed in a circle of radius 500 km at sea level around the sending station, which is located at the position of SwissOGS in Zimmerwald, Switzerland. The passes selected are shown in Fig. 2. The passes have been chosen to be at relatively high elevation culmination for the monostatic station to ensure all stations have long enough visibility. All receive only stations and the send station generate range measurements with the same gaussian noise of $\sigma_{mono} = \sigma_{bi} = 10m$ and clock-offsets of 0 s every 10 s. The magnitude of the noise was chosen to represent the noise to be expected from an object around 10 m in size like ENVISAT or a rocket stage [1]. While the clock-offset has been identified as an important parameter in bi- and multi-static SLR [2, 3], perfectly synchronized clocks are assumed in the following simulations.

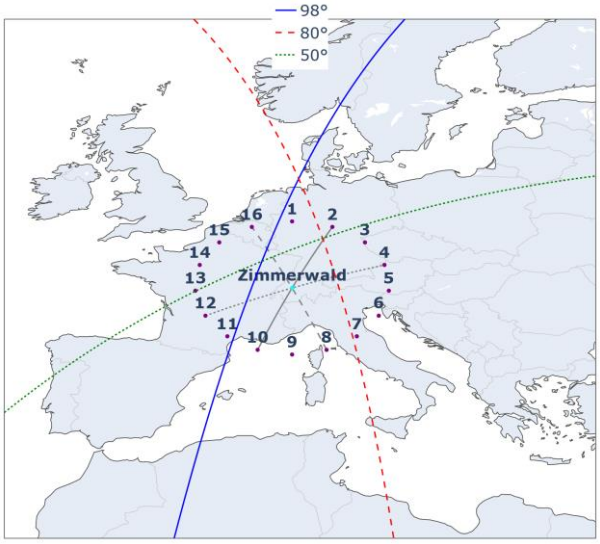

Figure 2: Position of Zimmerwald station and a ring of numbered bistatic stations (radius of 500 km). The geometries for the passes of different inclinations are highlighted.

3.1 Bistatic scenarios

Using this simulation setup, the mono- and bistatic range measurements are generated and used to perform orbit improvement. As a first test, the monostatic data from each pass is provided to the LSE. A full orbit estimate, i.e. estimating all Kepler orbital elements, is not possible from only one pass. This is to be expected, as only one pass usually results in normal equations which are not observable [2]. Observability can be achieved, by adding a second station from the ring, to contribute bistatic measurements to the orbit determination.

The passes are observed by all stations under different maximum elevations. Fig. 3 shows the 98° and 50° inclination passes observed by Zimmerwald and selected bistatic stations by plotting the RSOs azimuth and zenith angle. For Zimmerwald, the 98°, 80°, and

50° inclination passes culminate at 15.96°, 18.38°, and 19.47° respectively. It has to be noted, that the minimum possible zenith angle the telescope at SwissOGS (ZimLAT) is still able to track objects at, is about 10° for Low Earth Orbit (LEO) objects. This is caused by the alt-azimuth mounting of the telescope, which is not able to track near zenith due to limited tracking speeds.

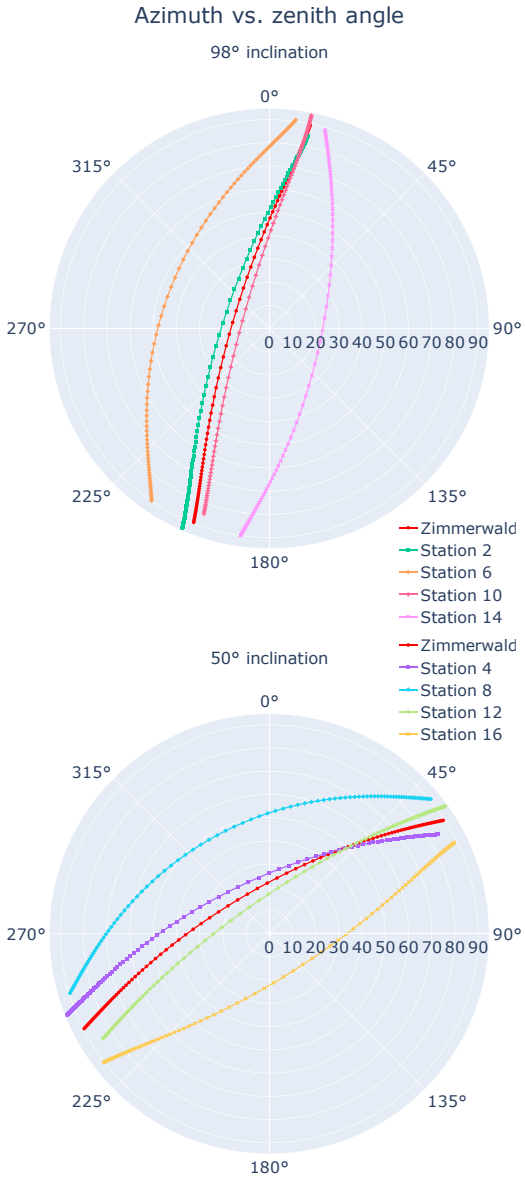

Figure 3: Azimuth and Zenith angle of passes of several selected stations

The absolute value of the difference between the estimated and true orbit evaluated at the initial measurement epoch is computed and plotted versus the station number in Fig. 4, to see which station geometry is most advantageous to estimate the orbit. Looking at the trace of the 98° inclination pass in Fig 4. shows the absolute error growing significantly for station 2 and 10 by up to two orders of magnitude. Furthermore stations 2 and 10 sit opposite of each other along the circle of stations. Drawing the baseline between Zimmerwald in Fig. 2 and a station on the high error axis reveals that the baseline is almost parallel to the orbital plane. This same trend also holds for the other passes with different axes respectively. As the axis is almost parallel to the orbital plane, a station on this axis will see the RSO under similar conditions as the sending station. Therefore, less new information can be contributed to the orbit determination. A station with a baseline angle closer to 90° will see the target from a different direction during the pass and can therefore observe movement components complementary to the sending station, increasing the orbit determination accuracy. Another factor to consider is the maximum elevation that is achieved during the pass. During low elevation passes the along track component is hard to estimate due to the unfavourable geometry, which leads to high orbit determination errors. This fact explains why the plots are not exactly symmetric around the high error axis: Stations which are further away from the RSO ground track observe at a lower elevation, which leads to higher orbit determination errors. To optimize the orbit determination performance of a bistatic scenario, a station baseline orthogonal to the orbital plane should be chosen. For (quasi-) polar orbits this suggests an east-west distribution of bistatic stations should be preferred.

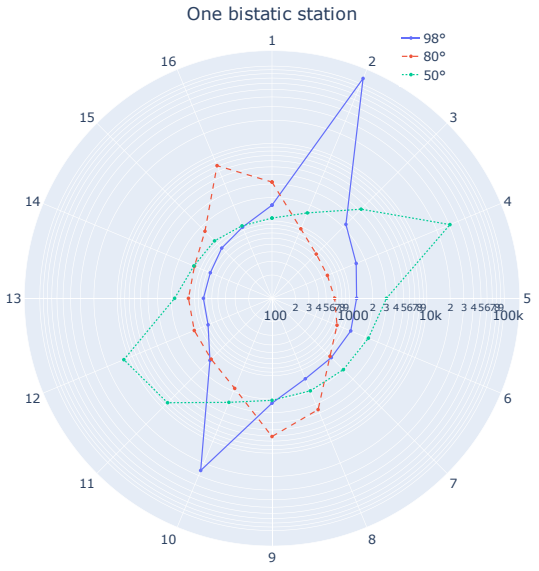

Figure 4: Mean absolute error in meters vs. station number for one bistatic station

3.2 Multistatic scenarios

Using the same ring of stations, the number of bistatic receive stations is increased to two. In the first case an offset of 90° between two stations is set. The resulting

error is shown in Fig. 5. While Fig. 4 shows a clear axis along which the error increases, adding another station makes the error less dependent on station directions. The resulting error plots show an almost circular shape, with a radius slightly smaller as the bistatic case. Furthermore, an asymmetry can be observed which can be explained by the different culmination elevations under which the passes are observed by different stations, with lower elevations leading to larger orbit determination errors.

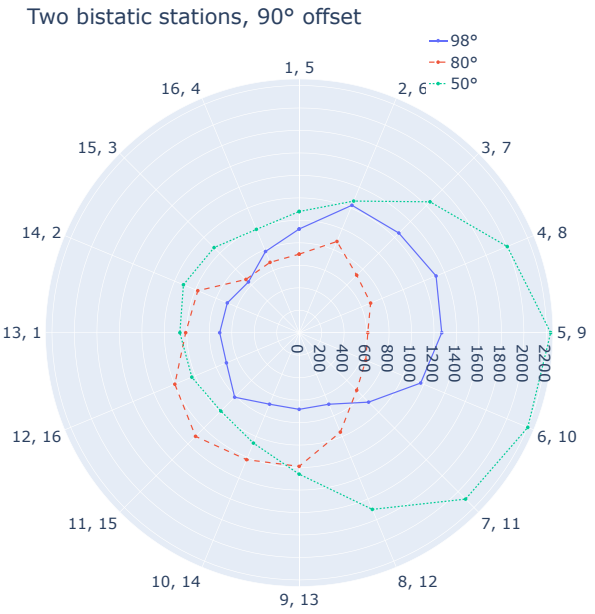

Figure 5: Mean absolute error in meters vs. station numbers for two bistatic stations, 90° offset.

As a second example, two receive stations with an offset of 180° are added to the sending station. The resulting error plot is shown in Fig. 6. Similar to Fig. 4 stations on the axis parallel to the orbital plane exhibit errors a magnitude larger, as the end-receive station baseline becomes parallel to the orbital plane. As opposite points on the plot correspond to the same pair of stations, this plot exhibits point-symmetry. Comparing the absolute values of the errors, the 180° configuration can outperform the 90° configuration if station baselines are orthogonal to the orbital plane, but are comparable for most other orientations.

In conclusion for the examined multistatic cases, an angle of 90° between receiving stations achieved the most robust results, irrespective of the baseline angles. While the 180° case sometimes leads to better accuracies, this comes at the cost of passes parallel to the station baseline leading to high errors in the orbit determination.

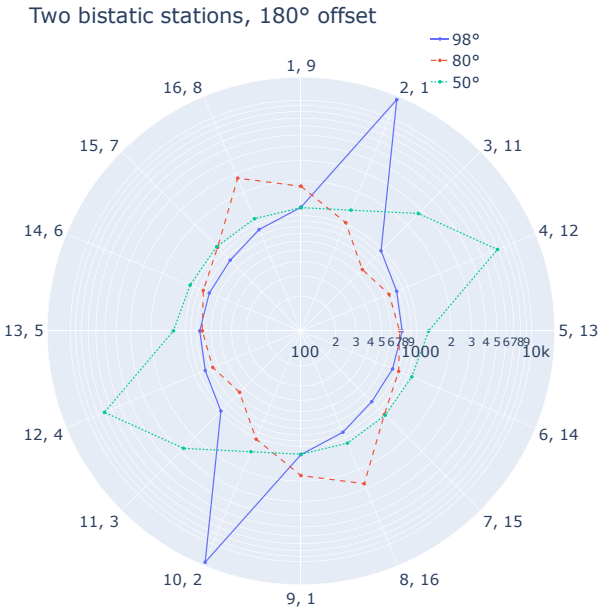

Figure 6: Mean absolute error in meters vs. station numbers for two bistatic stations, 180° offset.

3.3 Multistatic scenario: Zimmerwald-Graz-Herstmonceux

The previous scenarios have been utilizing a ring of fictitious stations around Zimmerwald. In reality no two existing SLR stations are exactly the same distance from this central station. However, the distance of the SLR stations Graz and Herstmonceux are around 610 km and 680 km from Zimmerwald. The angle between the baselines Herstmonceux-Zimmerwald and Zimmerwald-Graz of 132.1° also closely matches the angle of $6 \cdot 22.5° = 135°$ between station 15 and 5 in a circle scenario. Therefore, in this section a circle-scenario of 16 stations at sea-level with a radius of 640 km is performed and compared with a multistatic scenario of the real positions of Graz and Herstmonceux. A figure of the pass geometries is shown in Fig. 7.

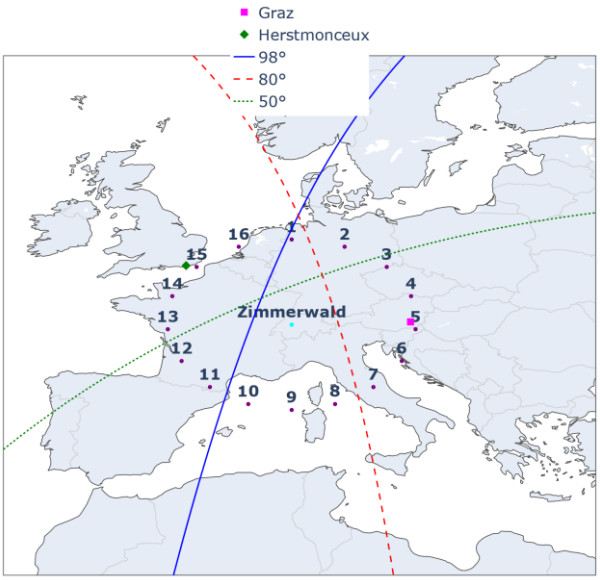

Figure 7: Position of Zimmerwald station and a ring of numbered bistatic stations (640 km). The passes of different inclinations, as well as the positions of Graz and Herstmonceux are highlighted.

Analogous to previous multistatic scenarios with two receiving stations, the mean absolute error is plotted versus the station numbers in Fig. 8. It can be noted that the plots are the same magnitude of the errors seen in Fig. 5, while still exhibiting an axis along which the error increases like in Fig. 6. This can be explained, by the baseline angle of 135° lying directly between 90° and 180°. The tracking geometry should therefore exhibit characteristics of both extremes. The axis along which the error increases, appears to be shifted by around 22.5° in comparison to the collinear case in Fig. 6. In addition to the plots of the circle stations, the error values for the Graz-Herstmonceux tracking scenario are marked as points near the station pair 5 and 15. While for the 98° inclination scenario the error values are in good agreement, while for the 80° and 50° inclination case there is a significant deviation between the values. As both all the points in the plot represent the mean of multiple simulation runs, the distribution of the runs has to be considered when deciding if they can be compared.

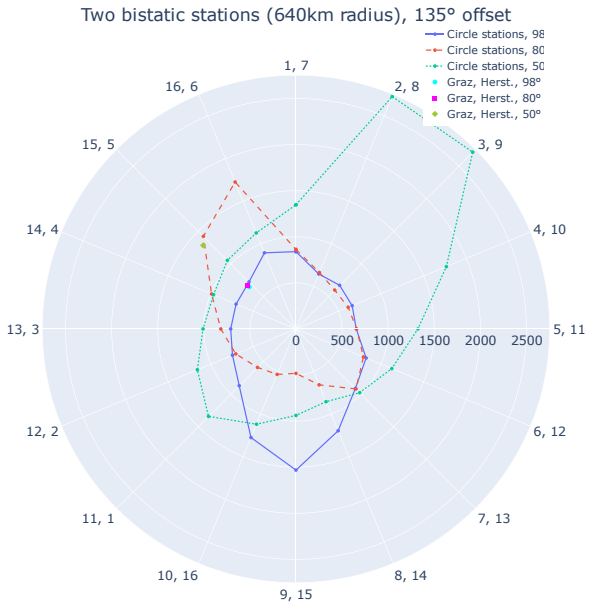

Figure 8: Mean absolute error in meters vs. station numbers for two bistatic stations, 135° offset. The mean absolute error for the station pair Graz-Herstmonceux displayed as points.

Fig. 9 shows the distribution of the absolute errors for station 15 and 4, as well as Graz and Herstmonceux in a box plot. The dashed line shows the mean value, while the uninterrupted line shows the median. Next to each box, the distribution of the actual data points is shown. For the 98° inclination pass, both cases are in good agreement, while for the 80° and 50° inclination pass the mean and median show a significant difference. To determine if this difference is also statistically significant, a two-sided Kolmogorov-Smirnov test for goodness of fit is performed. The confidence level is chosen at 95%, therefore the null-hypothesis, that the two distributions are identical, can be rejected for a p-value smaller than 5%. For the 98° inclination case a p-value of 0.47 is calculated, which means the null-hypotheses cannot be rejected. For the 80° and 50° cases a p-value of 0.000032 and 0.036 are calculated. The null-hypothesis is therefore rejected, which means the distributions are indeed different. One explanation why the circle tracking scenario is hard to compare to the real SLR-stations scenario can be seen when considering the bistatic scenarios of Zimmerwald-Graz and Zimmerwald-Herstmonceux in the context of Fig. 4. Graz is located slightly more north than station 5, which would place it between station 4 and 5 in Fig. . For the 98° inclination case this would not change the predicted error much, while for the 80° pass the error would decrease and increase for the 50° inclination case, as the angle between the station baseline and the orbital plane gets larger and smaller respectively. A similar argument

can be made for Herstmonceux's contribution. Another difference between the circle stations and the realistic stations that can influence the result is a different station elevation. The stations on the circle are considered to be at sea level while Graz SLR station is located 539 m and Herstmonceux station 75 m above sea-level. Higher elevations lead to shorter passes, which lead to less ranges being observed.

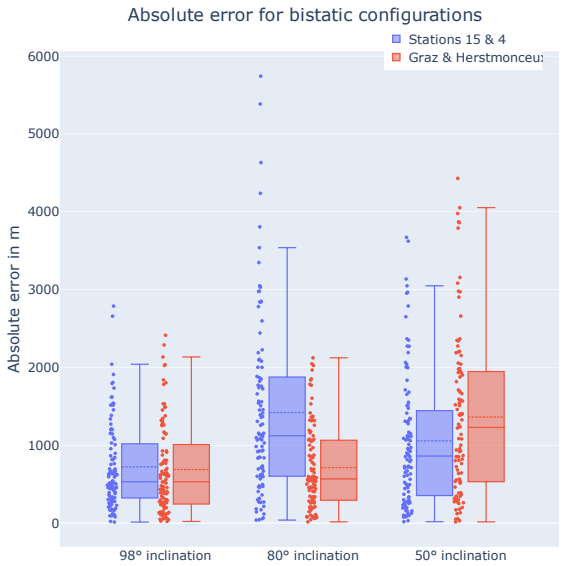

Figure 9: Boxplot visualizing the absolute error in m for the different orbit inclinations and for the circle scenario and the Graz-Herstmonceux scenario.

4 Conclusion

In this work a new simulation environment based on Orekit has been presented and scenarios of different bi- and multi-static tracking geometries have been shown. The simulator is capable to generate mono- and bi-static laser ranging signals, which are used for an orbit-determination procedure using least-squares estimation. The estimated orbits are then compared to the underlying ground-truth to learn how accurate the orbit determination is. Using this framework orbit improvement on a single pass of different inclination is explored for bistatic receive only stations located in circle around the sending station. The angle between the baseline of sending and receiving station and the orbital plane was identified as a critical parameter to predict how well the orbit is able to be determined. An angle of 90° led to the best results for the orbit improvement, which means an east-west distribution between stations is preferable for tracking polar orbits. Expanding the tracking network to two receive-only stations showed a decrease in uncertainty depending on the angle between the baselines of the stations as well as their relative position to the orbit. Finally, the stations Graz and Herstmonceux were used as an example to be examined in the previously established context. It could be shown that the previously discussed circle model applies for certain tracking geometries.

5 Acknowledgements

We acknowledge the funding from SNF under the project SNSF 200020_212181. We also thank Nicola Cimmino for the fruitful discussions.

6 References

1. Kirchner, G., Koidl, F., Ploner, M., Lauber, P., Utzinger, J., Schreiber, U., ... & Weigel, M. (2013, November). Multistatic laser ranging to space debris. In 18th International Workshop on Laser Ranging (pp. 13-0213).
2. Bamann, C., Hugentobler, U., Kirchner, G., Schreiber, U., Eckl, J., & Riepl, S. (2015, October). Analysis of Mono and Multi-static Laser Ranging Scenarios for Orbit Improvement of Space Debris. In *Proceedings of the 21st 25th International Symposium on Space Flight Dynamics ISSFD, Munich, Germany* (pp. 19-23).
3. Bamann, C., & Hugentobler, U. (2016). A Particle Filter for Orbit Determination of Space Debris based on Mono-and Multi-static Laser Ranging. In *Advances in the Astronautical Sciences, AAS/AIAA Space Flight Mechanics Meeting 2016*.
4. Wirnsberger, H., Baur, O., & Kirchner, G. (2015). Space debris orbit prediction errors using bi-static laser observations. Case study: ENVISAT. *Advances in Space Research*, *55*(11), 2607-2615.
5. Cordelli, E., Vananti, A., & Schildknecht, T. (2020). Analysis of laser ranges and angular measurements data fusion for space debris orbit determination. *Advances in Space Research*, *65*(1), 419-434.
6. Maisonobe, L., Pommier, V., & Parraud, P. (2010, May). Orekit: An open source library for operational flight dynamics applications. In *4th international conference on astrodynamics tools and techniques* (pp. 3-6). Paris: European Space Agency.